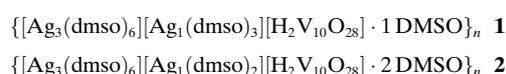# Communications

Supramolecular Silver Polyoxometalate Architectures Direct the Growth of Composite Semiconducting Nanostructures**

*Carsten Streb, Ryo Tsunashima, Donald A. MacLaren, Thomas McGlone, Tomoyuki Akutagawa, Takayoshi Nakamura, Antonino Scandurra, Bruno Pignataro, Nikolaj Gadegaard, and Leroy Cronin**

The controlled bottom-up assembly of nanostructured materials from molecular precursors has great promise if molecular synthetic control can be translated to the nanoscale.[1] This is because the assembly of molecules in the low-nanometer domain (0.5–5 nm) is possible by bottom-up molecular self-assembly[2] yet is not possible for top-down methods owing to the present limitations of lithography (ca. 10 nm). In our own work we have hypothesized[3] that linkable polyoxometalates (POMs) (anionic transition-metal-oxide clusters) have great potential to direct nanomaterial growth,[4] since POMs themselves are molecular, yet can approach 5 nm in size for the largest known cluster.[5] Although POMs have a host of applications,[6] they have not yet been extensively exploited as precursors for the formation of composite metal oxide nanostructures, because they first need to be linked into highly organized arrays. One of the most successful assembly methods to connect POM clusters involves the coordination of secondary transition metal species, thereby giving access to a range of molecular materials with diverse structures and properties.[7] In this respect we have been using silver-based linkers to generate POM-based 0-, 1-, 2-, and 3D frameworks using cation control, in which silver ions are ligated mainly in an oxo-based ligand environment.[8]

Herein, we demonstrate that it is possible to embed $\{Ag_3\}$ and $\{Ag_1\}$ units with $[H_2V_{10}O_{28}]^{4-}$ clusters into supramolecular architectures, giving compounds **1**, a 1D zigzag chain, and **2**, a 2D network (see Figure 1).

$\{[Ag_3(dmso)_6][Ag_1(dmso)_3][H_2V_{10}O_{28}] \cdot 1\,DMSO\}_n$ **1**

$\{[Ag_3(dmso)_6][Ag_1(dmso)_2][H_2V_{10}O_{28}] \cdot 2\,DMSO\}_n$ **2**

Furthermore, we show that these crystalline precursors can be utilized in a novel reactive-template route for the gram-scale production of composite semiconducting vanadium oxide nanowires incorporating discrete silver nanoparticles.[9] We also demonstrate that the crystalline long-range ordering of the precursors is an essential prerequisite for the nanostructure formation, as identical amorphous compounds do not yield the composite nanowires. The synthetic route for the nanowire production involves the simultaneous reduction and degradation of the silver polyoxovanadate precursors **1** or **2** to form a composite $Ag@VO_x$ nanowire system (**3**) in which metallic silver nanoparticles are embedded within a semiconducting vanadium oxide VO_x matrix.

Compounds **1** and **2** are two structurally closely related crystalline silver polyoxovanadate precursors that were developed to investigate their transformation into nanostructured composite materials. Compounds **1** and **2** were synthesized by the reaction of silver(I) nitrate with tetra-*n*-butylammonium decavanadate, $(nBu_4N)_3[H_3V_{10}O_{28}]$ in dimethyl sulfoxide (DMSO)/acetonitrile mixtures in 49% and 34% yield, respectively. Single-crystal X-ray diffraction analysis,[10] along with chemical analysis, and bond valence sum calculations allowed the formulae to be assigned. The crystallographic analysis of the materials showed that **1** and **2** feature virtually identical structural building blocks (Figure 1). Both contain diprotonated decavanadate clusters $[H_2V_{10}O_{28}]^{4-}$ (= $\{V_{10}\}$) as their main backbone, which are linked by linear trimeric silver(I) DMSO units $[Ag_3(dmso)_6]^{3+}$ (= $\{Ag_3\}$) binding to the cluster through coordinative Ag–O–V bonds. In addition, both compounds contain a monomeric silver(I) unit: In compound **1**, this $\{Ag_1\}_{cap}$ unit, $[Ag(dmso)_3]^+$, acts as a capping group, resulting in the formation of 1D supramolecular chains. In compound **2** however, the $\{Ag_1\}_{link}$ unit, $[Ag(dmso)_2]^+$, acts as a secondary linker between neighboring clusters and results in the formation of 2D networks (Figure 2).

[*] Dr. C. Streb, Dr. R. Tsunashima, T. McGlone, Prof. L. Cronin
WestCHEM, Department of Chemistry
The University of Glasgow
Glasgow G12 8QQ (UK)
Fax: (+44) 141-330-4888
http://www.chem.gla.ac.uk/staff/lee/index.html
E-mail: l.cronin@chem.gla.ac.uk

Dr. D. A. MacLaren
Department Physics and Astronomy, The University of Glasgow

Dr. N. Gadegaard
Department of Electronics and Electrical Engineering,
The University of Glasgow

Prof. T. Akutagawa, Prof. T. Nakamura
Research Institute for Electronic Science, Hokkaido University,
Sapporo, 001-0020 (Japan)

Dr. A. Scandurra
Superlab—Consorzio Catania Ricerche, Catania (Italy)

Prof. B. Pignataro
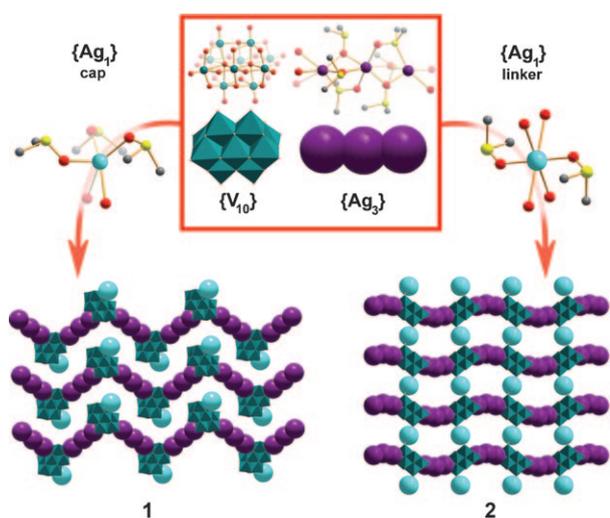Dipartimento di Chimica Fisica "F. Accascina", Università di
Palermo (Italy)

Figure 1. The structures of compounds **1** and **2**. Top center: the common building blocks {Ag$_3$} ($=$[Ag$_3$(dmso)$_6$]$^{3+}$) and {V$_{10}$} ($=$[H$_2$V$_{10}$O$_{28}$]$^{4-}$). Top left: {Ag$_1$}$_{cap}$ ($=$[Ag(dmso)$_3$]$^{1+}$) unit in **1**, shielding one cluster face from further interactions. Top right: {Ag$_1$}$_{link}$ ($=$[Ag(dmso)$_2$]$^{1+}$) unit in **2** linking two neighboring cluster units. Bottom: Formation of the 1D zigzag chains in **1** (left) and 2D planar networks in **2** (right). Ag purple or light blue, V green, O red, C gray, S yellow, {V$_{10}$} green polyhedra, {Ag$_3$} purple spheres, {Ag1}$_{cap/link}$ light blue spheres.

A novel reactive-building-block synthesis was then used to investigate the controlled nanostructure formation from the crystalline single-source precursors **1** and **2**. The reduction of compounds **1** or **2** with hydrazine in a water/DMSO mixture proceeds identically for both compounds and resulted in the complete conversion of **1** or **2** into composite **3** (Scheme 1).

Scanning electron microscopy (SEM) micrographs showed that composite **3** is entirely composed of extensively cross-connected and interweaved nanowires, resulting in a nanostructured material that can be described as a nanomesh (Figure 3). The wires have uniform diameters of 20–30 nm and maximum lengths of over 4 μm, giving high aspect ratios in excess of 200. The most prominent connectivity feature of the wires is a "splitting and merging" motif where a set of two or more wires are intimately connected and run parallel for several hundred nanometers before splitting up into single
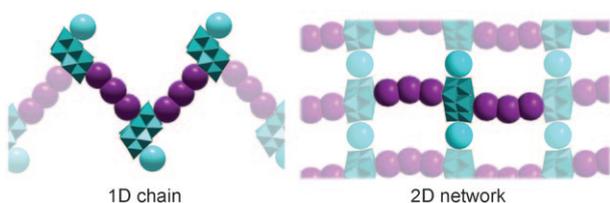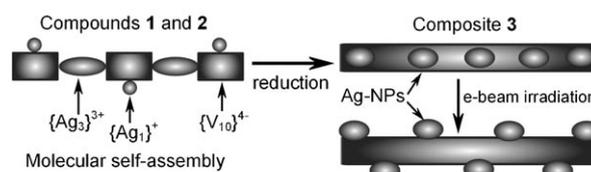

Figure 2. Detailed schematic representation of the supramolecular architectures in **1** and **2**. Left: 1D zigzag chains in compound **1** formed by coordination of {Ag$_3$} linker groups to adjacent faces of the {V$_{10}$} clusters with capping {Ag$_1$}$_{cap}$ groups. Right: Planar 2D network in compound **2** where {V$_{10}$} clusters are cross-linked by {Ag$_3$} primary linkers and secondary {Ag$_1$}$_{link}$ units. {V$_{10}$} green polyhedra, {Ag$_3$} purple spheres, {Ag$_1$}$_{cap/link}$ light blue spheres.

Scheme 1. The one-step transformation of crystalline precursors into composite Ag@VO$_x$ wires. Crystalline polymeric arrays of [H$_2$V$_{10}$O$_{28}$]$^{4-}$ units and [Ag$_3$]$^{3+}$/[Ag]$^{+}$ groups found in compounds **1** and **2**, are transformed into the nanostructured composite **3**. Under TEM-conditions, the silver NPs are ejected from the Ag@VO$_x$ wire matrix.
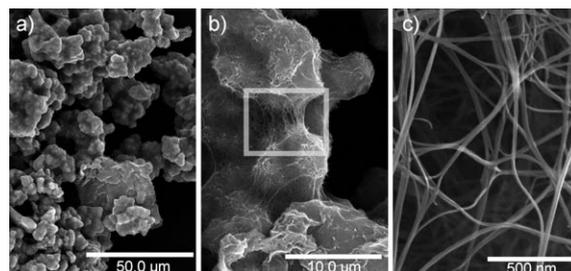

Figure 3. SEM micrographs of the nanowire structures in composite **3**. a) Low magnification micrograph showing the globular superstructures of cross-connected wires and their assembly into large aggregates. b) Detailed illustration of the highly cross-linked globular wire superstructures which are connected by sections of aligned wires (highlighted by a gray rectangle). c) High resolution micrograph of a globule section, showing the highly interweaved structure and the splitting and merging of the wire strands which leads to their macroscopic aggregation.

strands which continue their growth in different directions and subsequently merge with other wire strands (Figure 3c). This feature results in a highly interweaved structure which is reflected by the macroscopic aggregation of **3**. The wires assemble into interconnected globular superstructures with typical diameters of approximately 5 μm which are made up of a multitude of highly cross-linked wire strands. These globular wire superstructures are cross-connected by sections of aligned wire strands which extend between adjacent globules (Figure 3b). The fabric-like interweaving on the nanoscale is reflected by the mechanical stability of the bulk compound, and these aggregates can be fabricated into robust monoliths of various shapes (see Supporting Information, Figure S1). This assembly of nanowires into highly connected superstructures is in stark contrast to other metal oxide nanowires, which are often obtained as highly dispersed or colloidal systems.[11] One advantage of these nanostructured macroscopic aggregates is the facile separation from a liquid, as the bulk material settles quickly to the bottom of a vessel. This feature is desirable in applications such as heterogeneous catalysis,[9] where facile separation of the solid catalyst from the reaction mixture is critical. In addition, nitrogen sorption measurements of **3** verified the full accessibility of the wire surfaces and gave a BET specific surface area of 24.7 m^{2}g^{-1}.

Powder X-ray diffractometry (XRD) of the as-synthesized composite **3** indicated that the nanowires contain face-

centered cubic (fcc) silver metal. Transmission electron microscopy (TEM) studies verified the presence of silver as metallic silver nanoparticles, with diameters of 5-25 nm, embedded in an amorphous vanadium oxide matrix (Figure 4). Further, electron diffraction studies allowed the
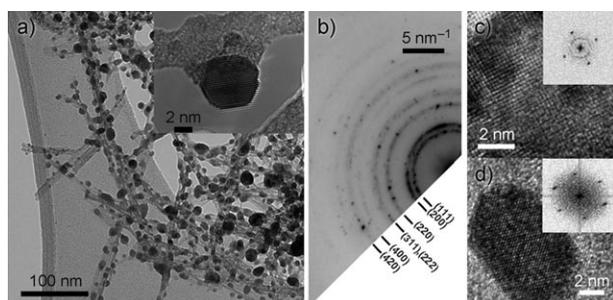

Figure 4. TEM and electron diffraction images of the composite nanowires in **3**. a) Bright-field TEM of the composite Ag@VO$_x$ wires. Inset: High-resolution TEM of an Ag nanoparticle embedded in the nanowire matrix. b) Electron diffraction pattern of a similar area, indicating rings consistent with the fcc silver metal. No strong diffraction from the amorphous matrix was observed. c) A typical region of the reduced vanadium matrix after exposure to the electron beam. Inset: Fourier transform consistent with a body-centered cubic (bcc) symmetry, giving a lattice constant of $a_V = 2.87$ Å. d) A crystalline silver nanoparticle. Inset: Fourier transform consistent with a face-centered cubic (fcc) symmetry and a lattice constant of $a_{Ag} = 3.91$ Å.

unambiguous identification of the nanoparticles as crystalline face-centered cubic (fcc) silver metal with a lattice constant of $a_{Ag} = 3.91$ Å, thereby confirming the initial bulk powder XRD study.[12] Also, under typical TEM conditions, it was observed that the electron beam reduces the original amorphous vanadium oxide wire and sections of the nanowire matrix showed crystalline ordering consistent with body centered cubic (bcc) vanadium metal with a lattice constant of $a_V = 2.87$ Å (Figure 4c).[12] This reduction process also explains why the silver nanoparticles were not observed in the initial SEM study: the silver nanoparticles are enclosed inside the VO$_x$ matrix giving an inorganic Ag-in-VO$_x$ peapod (c.f. organic carbon nanotube systems),[13] which is stable under SEM conditions, in which the sample is also coated by gold through sputtering. This observation is further verified by the high mechanical stability of the silver nanoparticle/vanadium oxide interface. Prolonged sonicating and mechanical agitation resulted in the breakage of the wire aggregates into smaller sections, however, no separation of the silver metal nanoparticles from their surrounding VO$_x$ matrix was observed.

The electronic structure of the composite was investigated using x-ray photoelectron spectroscopy (XPS) which showed the presence of oxygen together with reduced vanadium species and fully oxidized vanadium(V) centers, giving a molar ratio of oxidized to reduced vanadium atoms of $V_{oxidized}/V_{reduced} = 1.90$. This result allows verification of the proposed matrix composition as non-stoichiometric mixed oxidation state VO$_x$, vanadium oxide.[14] Although XPS studies do not allow the unambiguous distinction between vanadium centers in oxidation states V^{IV} or V^{III}, arguments based upon redox-

potential considerations mean that the reduced vanadium species can be tentatively assigned as V^{IV}, consistent with previous reports.[14] The presence of reduced vanadium species is vital for the electronic properties of the vanadium oxide matrix as they allow fine-tuning the conductivity of the material and bulk conductivity measurements of composite **3** showed that the material behaves as a room-temperature semiconductor. High conductivities of 0.156 S cm^{-1} were observed at 273 K which corresponds well to the large number of reduced vanadium centers observed by XPS. A small polaron hopping theory model[14] was applied to estimate the activation energy of 0.14 eV at the transition temperature $T = 150$ K. These electronic features are in line with similar V$_2$O$_5$-based nanowire systems[14] and further support the characterization of the wire matrix as a mixed valence VO$_x$-type metal oxide.

A comparative study was undertaken to gain some insight into the critical synthetic parameters of the nanowire formation, as initial experiments suggested that the crystallinity of the precursors **1** and **2** might be essential for the successful production of the Ag@VO$_x$ nanowires. A range of amorphous precursors (powders, pellets, amorphized crystals) of identical composition were therefore deliberately synthesized by carefully desolvating crystals of **1** or **2** at increased temperature and the materials were treated under identical synthetic conditions to evaluate the importance of an intact crystal matrix for the nanowire production. All amorphous samples failed to produce the Ag@VO$_x$ nanowires. Instead, non-uniform microparticles with irregular structures and compositions were obtained (see Supporting Information, Figure S12). To evaluate whether the nanowire growth occurs at the solid/liquid interface, or is purely a liquid-phase reaction, the original mother liquor from which the crystals of **1** and **2** are obtained was directly employed in the reduction/degradation reaction. In this case, it was observed that the reaction resulted in the direct reduction of the silver(I) ions to yield polydisperse metallic silver particles which subsequently aggregated into larger agglomerates. Interestingly, the vanadate precursors remained solubilized in the reaction solution and no vanadate-based solids were detected at all.

In summary, a novel POM-based approach for the controlled synthesis of composite metal/metal oxide nanostructures has been presented, in which the crystalline precursors are selectively transformed into nanoscopic wires with metallic silver particles embedded into an amorphous vanadium oxide nanowire matrix. The procedure has significant advantages over existing nanowire/nanoparticle syntheses as it allows the grafting of metal nanoparticles directly onto a catalytically active metal oxide nanowire matrix in a facile, one-step, room-temperature process that gives materials on a gram scale. The large number of available transition-metal POM compounds, with a range of different and configurable properties, means that there is real prospect for preparing complex nanostructured materials using this process. Further, the fabrication of composite catalysts can be envisaged in which the distinctive properties of the nanoparticles and the matrix can be combined to give a one-pot, two-component system on the nanoscale.

Experimental Section

Detailed syntheses of compounds **1–3** can be found in Supporting information. Compounds **1** and **2** are synthesized by reaction of $(n\text{Bu}_4\text{N})_3[\text{H}_3\text{V}_{10}\text{O}_{28}]$ with AgNO_3 in DMSO/acetonitrile mixtures at different $\{\text{V}_{10}\}/\text{Ag}$ ratios. The materials were crystallized by diffusion of ethyl acetate into the reaction mixtures. For **3**, crystals of **1** or **2** were removed from the mother liquor, washed with cold ethanol, briefly air-dried and immersed in a 1:1 (v:v) mixture of 5 M aqueous hydrazine hydrate and DMSO. The initially orange/red crystals changed color to dark gray/black and were subsequently washed with water and ethanol to remove any DMSO and hydrazine residue. Subsequent washing with deionized water to remove soluble vanadate compounds yielded composite **3** as fibrous aggregates in ca. 48 wt.% yield.

[1] A. R. Pease, J. O. Jeppesen, J. F. Stoddart, Y. Luo, C. P. Collier, J. R. Heath, *Acc. Chem. Res.* **2001**, *34*, 433–444.

[2] S. A. Barnett, N. R. Champness, *Coord. Chem. Rev.* **2003**, *246*, 145–168.

[3] D.-L. Long, L. Cronin, *Chem. Eur. J.* **2006**, *12*, 3698–3706; D.-L. Long, E. Burkholder, L. Cronin, *Chem. Soc. Rev.* **2007**, *36*, 105–121.

[4] T. Liu, *J. Am. Chem. Soc.* **2003**, *125*, 312–313.

[5] A. Müller, E. Beckmann, H. Bögge, M. Schmidtmann, A. Dress, *Angew. Chem.* **2002**, *114*, 1210–1215; *Angew. Chem. Int. Ed.* **2002**, *41*, 1162–1167.

[6] a) J. T. Rhule, C. L. Hill, D. A. Judd, *Chem. Rev.* **1998**, *98*, 327–357; b) C. Fleming, D.-L. Long, N. Mcmillan, J. Johnston, N. Bovet, V. Dhanak, N. Gadegaard, P. Kögerler, L. Cronin, M. Kadodwala, *Nat. Nanotechnol.* **2008**, *3*, 229–233; c) A. Müller, F. Peters, M. T. Pope, D. Gatteschi, *Chem. Rev.* **1998**, *98*, 239–271; d) Y. V. Geletii, B. Botar, P. Kögerler, D. A. Hillesheim, D. G. Musaev, C. L. Hill, *Angew. Chem.* **2008**, *120*, 3960–3963; *Angew. Chem. Int. Ed.* **2008**, *47*, 3896–3899; e) J. Lehmann, A. Gaita-Arino, E. Coronado, D. Loss, *Nat. Nanotechnol.* **2007**, *2*, 312–314.

[7] a) C. Ritchie, E. Burkholder, P. Kögerler, L. Cronin, *Dalton Trans.* **2006**, 1712–1714; b) C. Ritchie, C. Streb, J. Thiel, S. G. Mitchell, H. N. Miras, D.-L. Long, T. Boyd, R. D. Peacock, T. McGlone, L. Cronin, *Angew. Chem.* **2008**, *120*, 6987–6990; *Angew. Chem. Int. Ed.* **2008**, *47*, 6881–6884; c) C. Streb, C. Ritchie, D.-L. Long, P. Kögerler, L. Cronin, *Angew. Chem.* **2007**, *119*, 7723–7726; *Angew. Chem. Int. Ed.* **2007**, *46*, 7579–7582.

[8] a) Y. F. Song, H. Abbas, C. Ritchie, N. McMillian, D.-L. Long, N. Gadegaard, L. Cronin, *J. Mater. Chem.* **2007**, *17*, 1903–1908; b) H. Abbas, C. Streb, A. L. Pickering, A. R. Neil, D.-L. Long, L. Cronin, *Cryst. Growth Des.* **2008**, *8*, 635–642; c) H. Abbas, A. L. Pickering, D.-L. Long, P. Kögerler, L. Cronin, *Chem. Eur. J.* **2005**, *11*, 1071–1078; d) E. F. Wilson, H. Abbas, B. J. Duncombe, C. Streb, D.-L. Long, L. Cronin, *J. Am. Chem. Soc.* **2008**, *130*, 13876–13884.

[9] a) P. V. Kamat, *J. Phys. Chem. B* **2002**, *106*, 7729–7744; b) C. R. Xiong, A. E. Aliev, B. Gnade, K. J. Balkus, *ACS Nano* **2008**, *2*, 293–301; c) M. W. Shao, L. Lu, H. Wang, S. Wang, M. L. Zhang, D. D. D. Ma, S. T. Lee, *Chem. Commun.* **2008**, 2310–2312; d) G. C. Li, K. Chao, C. S. Ye, H. R. Peng, *Mater. Lett.* **2008**, *62*, 735–738; e) S. Sharma, M. Panthofer, M. Jansen, A. Ramanan, *Mater. Chem. Phys.* **2005**, *91*, 257–260; f) C. Marchal-Roch, C. R. Mayer, A. Michel, E. Dumas, F.-X. Liu, F. Sécheresse, *Chem. Commun.* **2007**, 3750–3752; g) D. Graham, D. G. Thompson, W. E. Smith, K. Faulds, *Nat. Nanotechnol.* **2008**, *3*, 548–551; h) M. P. Suh, H. R. Moon, E. Y. Lee, S. Y. Jang, *J. Am. Chem. Soc.* **2006**, *128*, 4710–4718.

[10] Crystallographic data and structure refinements for compound **1**: $\text{C}_{20}\text{H}_{62}\text{Ag}_4\text{O}_{38}\text{S}_{10}\text{V}_{10}$, $M_\text{r} = 2172.18 \text{ g mol}^{-1}$; block crystal: $0.40 \times 0.31 \times 0.25 \text{ mm}^3$; $T = 150(2)$ K. Monoclinic, space group $P2_1$, $a = 10.8165(2)$, $b = 22.5042(4)$, $c = 12.6180(2)$ Å, $\beta = 91.113(2)$, $V = 3070.85(9)$ Å^3, $Z = 2$, $\rho = 2.243 \text{ g cm}^{-3}$, $\mu(\text{Mo}_{\text{K}\alpha}) = 3.137 \text{ mm}^{-1}$, $F(000) = 1944$, 14382 reflections measured, 10177 unique ($R_\text{int} = 0.022$), 739 refined parameters, $R1 = 0.0266$, $wR2 = 0.0578$. Compound **2**: $\text{C}_{20}\text{H}_{62}\text{Ag}_4\text{O}_{38}\text{S}_{10}\text{V}_{10}$, $M_\text{r} = 2172.18 \text{ g mol}^{-1}$; block crystal: $0.30 \times 0.25 \times 0.22 \text{ mm}^3$; $T = 150(2)$ K. Monoclinic, space group $C2/c$, $a = 23.2469(6)$, $b = 11.2516(3)$, $c = 23.2770(6)$ Å, $\beta = 95.121(2)$, $V = 6064.1(3)$ Å^3, $Z = 4$, $\rho = 2.379 \text{ g cm}^{-3}$, $\mu(\text{Mo}_{\text{K}\alpha}) = 3.157 \text{ mm}^{-1}$, $F(000) = 4256$, 15309 reflections measured, 5614 unique ($R_\text{int} = 0.0399$), 432 refined parameters, $R1 = 0.0594$, $wR2 = 0.1186$. Crystal data were measured on a Oxford Diffraction Gemini S Ultra diffractometer using $\text{Mo}_{\text{K}\alpha}$ radiation ($\lambda = 0.71073$ Å) at 150(2) K. CCDC 724259 (**1**) and CCDC 724260 (**2**) contain the supplementary crystallographic data for this paper. These data can be obtained free of charge from The Cambridge Crystallographic Data Centre via www.ccdc.cam.ac.uk/data_request/cif.

[11] a) J. Muster, G. T. Kim, V. Krstic, J. G. Park, Y. W. Park, S. Roth, M. Burghard, *Adv. Mater.* **2000**, *12*, 420–424; b) Y. Zhang, F. Yang, J. Yang, Y. Tang, P. Yuan, *Solid State Commun.* **2005**, *133*, 759–763; c) Z. Kang, E. Wang, M. Jiang, S. Lian, *Nanotechnology* **2004**, *15*, 55–58.

[12] *The Cambridge Handbook of Physics Formulas*, 6th ed., Cambridge University Press, New York, **2006**.

[13] A. N. Khlobystov, K. Porfyrakis, M. Kanai, D. A. Britz, A. Ardavan, H. Shinohara, T. J. S. Dennis, G. A. D. Briggs, *Angew. Chem.* **2004**, *116*, 1410–1413; *Angew. Chem. Int. Ed.* **2004**, *43*, 1386–1389.

[14] a) J. Bullot, P. Cordier, O. Gallais, M. Gauthier, J. Livage, *Phys. Status Solidi A* **1981**, *68*, 357–361; b) J. Livage, *Chem. Mater.* **1991**, *3*, 578–593; c) J. Muster, G. T. Kim, V. Kristić, J. G. Park, Y. W. Park, S. Roth, M. Burghard, *Adv. Mater.* **2000**, *12*, 420–424.